Int. J. Electrochem. Sci., 15 **(2020)** 10584 – 10615, doi: 10.20964/2020.10.16

International Journal of ELECTROCHEMICAL SCIENCE
www.electrochemsci.org

Mini Review

Research Progress of Magnesium Anode Materials and Their Applications in Chemical Power Sources

Dong Jia[1], *Fan Liu*[1], *DongZi Yang*[1],*Wei Wang*[1, 2,*]

[1] School of Chemical Engineering and Technology, Tianjin University, Tianjin, China
[2] Key Laboratory of Metal Fuel Cell of Sichuan Province, Sichuan, China
[*] E-mail: wangweipaper@163.com

Received: 27 May 2020 / *Accepted:* 1 August 2020 / *Published:* 31 August 2020

With the growing demand for energy, it has become a topic of constant concern to find a new and environmentally friendly material for chemical energy supply. Magnesium, in addition to being a structural metal, is also a desirable and promising anode material used for chemical power supplies. This metal shows favorable characteristics such as highly negative electrode potential, high theoretical specific charge capacity and high theoretical energy density when used as anode materials. Its abundance on the earth and environmental friendliness also make magnesium more suitable for widespread use. However, there still exist several inherent disadvantages like product adhesion, voltage hysteresis, negative difference effect and self-discharge, which adversely affect and seriously restrict the use and development of magnesium as an anode material. In this paper, the research progress and applications of magnesium anode materials in recent years are reviewed in detail, the methods to improve the electrochemical performance and corrosion resistance of magnesium anodes are systematically introduced and the development trend of magnesium anode materials is prospected.

Keywords: magnesium anode, anodic efficiency, discharge activity, self-corrosion, first-principles

1. INTRODUCTION

The continuous progress of human society is closely related to the development and utilization of various resources. Today, the global energy crisis and environmental pollution problems become worse and worse [1]. Magnesium, in addition to being used as a structural metal material [2-5], has also attracted considerable interest and attention in the field of chemical power sources because of its negative standard electrode potential (-2.37 V vs. standard hydrogen electrode (SHE)), high theoretical specific energy (2.2 Ah g^{-1}) and high theoretical energy density (3.8 Ah cm^{-3}) [6-10]. Besides, low density (1.74 g cm^{-3}), which can reduce the overall weight of the batteries [11], environmental friendliness and abundant reserves also make magnesium a promising electrode material [12].

As is known to all, chemical power sources usually adopt the active metal as anode for current generation. The active metal loses electrons and dissolves into the electrolyte, and then the oxidant obtains the electrons at the cathode and is reduced, generating the electric current. Therefore, the selection of metal anode material plays an important role in the properties of the power sources [13, 14]. Magnesium happens to be this kind of suitable active metal due to the aforementioned inherent advantages and has been widely used as an ideal anode material in varieties of chemical power supplies.

In this paper, the applications of magnesium anodes in different kinds of chemical power supplies and their respective working principles are summarized. Some theoretical and practical methods to improve the electrochemical and corrosion performance of magnesium anodes and the corresponding mechanism are introduced, respectively. In the end, it points out the shortcomings of the existing research and proposes the future research direction of magnesium alloy anodes [15].

2. APPLICATIONS OF MAGNESIUM ANODES IN CHEMICAL POWER SUPPLIES

As promising anode material used in chemical power supplies, magnesium exhibits many inherent advantages that other materials do not have such as a negative electrode potential of -2.37 V (vs.SHE) to promise high discharge activity, high theoretical specific energy (2.2 Ah g^{-1}) and high theoretical energy density (3.8 Ah cm^{-3}) [7-10]. All these advantages make it a widely studied material in the field of chemical power sources. Besides, low density, abundant resources and low environmental pollution make it more advantageous and competitive than other materials [16-18].

Naturally, with so many competitive advantages, magnesium has been widely used as anode material for various chemical power supplies, including metal-air batteries, seawater batteries, hydrogen peroxide semi-fuel cells, primary batteries, secondary batteries and so on, which cover both military and civilian aspects. The following are detailed introductions to various types of batteries with magnesium as the anode.

2.1 Air batteries

Metal-air batteries (MABs) are a kind of special fuel cells, which have aroused considerable interest as promising chemical power supplies due to the aforementioned advantages such as high energy density and low cost [19-21]. They usually adopt the active metal as the anode, the inert electrode as the cathode, and the neutral solution (such as NaCl) or alkaline solution (such as KOH or NaOH) as the electrolyte. When discharged, the metal anode dissolves and loses electrons and oxygen in the air is reduced on the cathode. Through the process of losing and gaining of electrons, the electric current is thus generated [22].

Based on this principle, for a metal-air battery whose discharge performance and actual capacity are mainly determined by the anode, the selection of anode material is therefore a significant subject. In the past few decades, Al-air and Zn-air batteries have been extensively explored [23-26], while Mg-air batteries have not been researched as much. Magnesium, for all its inherent advantages, is being further

studied by researchers as an anode material. The basic structure of a common Mg-air battery is shown in Fig. 1. The electrode and total reactions involved in the discharge process are written as:

$$Anode: Mg \rightarrow Mg^{2+} + 2e^{-}$$
$$Cathode: O_2 + 2H_2O + 4e^{-} \rightarrow 4OH^{-}$$
$$Total: 2Mg + O_2 + 2H_2O \rightarrow 2Mg(OH)_2$$

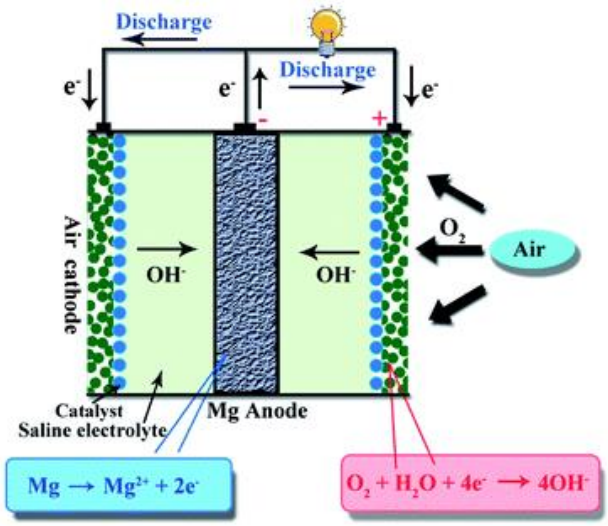

Figure 1. Basic structure and discharge principle of a Mg–air battery [6].

During the discharge process, Mg loses two electrons to be Mg^{2+}, and oxygen gains electrons at the inert electrode and is thus reduced to OH^-. The theoretical voltage provided by the Mg-air battery is 3.1 V [27]. Despite the high theoretical voltage, in fact, the practical voltage a Mg-air battery could provide is relatively low. There still exist some problems that restrict the widespread use of Mg-air batteries. Firstly, highly negative electrode potential of Mg promises itself high discharge activity, but consequent self-corrosion reaction leads to low utilization efficiency of the magnesium anode. Secondly, the reaction produces a relatively dense passivation film $Mg(OH)_2$, which affects the active dissolution of Mg, resulting in voltage hysteresis and low voltage.

To solve the contradiction between activation and passivation, many researches have been carried out to develop magnesium anode materials with both high discharge activity and simultaneous low corrosion rate.

Li et al. [28] developed a Mg-9%Al-1%In (AI91) alloy anode for Mg-air batteries. Mg-9%Al (A9) alloy and Mg-9%Al-1%Zn (AZ91) alloy were simultaneously prepared as comparison. The discharge behavior of the three alloys was investigated by potentiodynamic polarization and constant current discharge tests. In the potentiodynamic polarization test, AI91 alloy showed the most negative corrosion potential (E_{corr}) but the smallest corrosion current density (i_{corr}). As is known, negative corrosion potential means good discharge activity while small corrosion current density demonstrates good corrosion resistance. It could be inferred that the addition of indium restrained hydrogen evolution reaction due to the high hydrogen evolution over-potential of indium. The Mg-air battery performance

was tested at different current densities (2.5~50 mA cm^{-2}) via galvanostatic discharge tests. The small current densities were applied to study the discharge performance of the anode for long-duration and low-power devices while the large densities for the high-power applications. Under all current densities, the battery voltage decreased with the increase of impressed current density and the voltage of Mg-air battery assembled with AI91 anode was higher than that of others at all current densities. Besides, Mg-air battery with AI91 anode displayed highest anodic utilization efficiency and energy density when the applied current density was 40 mA cm^{-2}. According to the microstructure characterization and surface analyses, the addition of indium homogenized the distribution of the second phase (β-$Mg_{17}Al_{12}$) and the microstructure of AI91 alloy was refined. Besides, the discharge products of AI91 were the least dense and allowed more electrolyte to penetrate, promising better discharge performance.

Yuan et al. [29] prepared a Mg-3%Al alloy modified with Ga, In, Sn and investigated the electrochemical performance. Mg-3%Al-1%Sn (AS31), Mg-3%Al-1%Ga (AG31) and Mg-3%Al-1%In (AI31) alloys were prepared and Mg-3%Al (A3), common Mg-3%Al-1%Zn (AZ31) were also prepared for contrast. The potentiodynamic polarization results showed that A3 alloy had the most negative potential but it performed a drastic anodic polarization, the addition of alloying Ga, In, Sn weakened the polarization. Besides, the self-corrosion rate was decreased with the addition of Ga, In, Sn due to their small exchange current density (j_0) for the hydrogen evolution reaction[30]. The battery performance was tested after assembled with commercial air electrodes as cathodes. In this work, small current densities were applied to study the long-time discharge performance while larger current density to examine the discharge performance for short-term and high-power battery system. The results showed that the voltage of Mg-air battery with AI31 alloy was the highest among all assembled batteries at any current densities, and the discharge process was more stable. The assembled battery with AI31 anode acquired higher voltage and anodic utilization efficiency at small current density. When discharged at 10 mA cm^{-2}, the energy density of the Mg-air battery with AI31 alloy anode reached the maximum, meaning the AI31 alloy was more suitable for low-power applications.

2.2 Seawater batteries

Seawater batteries (SWBs) are a new type of chemical power sources which take seawater as infinite electrolyte and convert chemical energy into electric energy [31]. Seawater, covering two-thirds of the earth surface, is the most abundant natural resource on the earth. The use of seawater to obtain electricity is of significant interest today. At present, common seawater batteries include seawater activated batteries and seawater dissolved oxygen batteries.

2.2.1 Seawater activated batteries

Seawater activated batteries were firstly developed to satisfy the demand of military and defense devices [32], such as sonobuoys, torpedoes and meteorological radiosondes [33]. Generally, this type of battery consists of three parts. It takes active metals as anode, metal chlorides as cathode, and flowing seawater as electrolyte [34-36]. Therefore, there is no need to carry electrolyte and extra storage and

control device, simplifying the battery structure, reducing the weight of the battery, and increasing the unit energy density directly. The temperature of the battery is controlled by using naturally circulating seawater as an electrolyte, removing the electrode products while also taking away some of the heat released by the battery reaction [37]. In this battery system, the active metal is usually magnesium with a negative electrode potential. The typical structure of a common seawater activated battery is depicted in Fig. 2.

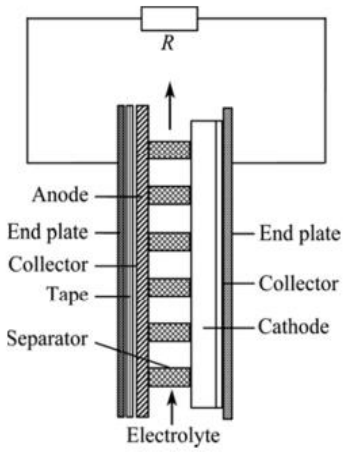

Figure 2. Typical structure of a seawater activated battery [15].

Among the common seawater batteries, Mg/AgCl batteries were firstly developed by Bell Telephone Laboratories for the power supply of military torpedoes [15]. This type of batteries could operate at relatively large current density and provide high energy density of 88 Wh kg^{-1}. Besides, it can be stored and used in a wide temperature range [38, 39]. Unfortunately, high cost of silver chloride limited the widespread use of this battery. The electrode and total reactions are as follows:

$$Anode: Mg \rightarrow Mg^{2+} + 2e^{-}$$

$$Cathode: 2AgCl + 2e^{-} \rightarrow 2Ag + 2Cl^{-}$$

$$Total: Mg + 2AgCl \rightarrow 2Ag + MgCl_2$$

Mg/CuCl battery is another kind of common seawater battery and was firstly developed by the former Soviet Union [32]. Compared with Mg/AgCl battery, the advantage of Mg/CuCl battery is that the battery is significantly cheaper because of the replacement of expensive AgCl by CuCl. However, this substitution also brings about problems, as it provides lower energy density and specific energy, and cannot be stored in wet environments for long periods. In addition, the oxidation of CuCl cathode must be prevented by the addition of tin chloride or argon, which also restricts its further application as deep-sea power source [40]. The electrode and total reactions are as follows:

$$Anode: Mg \rightarrow Mg^{2+} + 2e^{-}$$

$$Cathode: 2CuCl + 2e^{-} \rightarrow 2Cu + 2Cl^{-}$$

$$Total: Mg + 2CuCl \rightarrow 2Cu + MgCl_2$$

In summary, what these seawater activated batteries have in common is that they have a high cathode current density, and can provide high power but have a relatively short service life. They are generally used as high-power power seawater batteries and mainly used in sonar, torpedo and underwater propeller of large detection equipment. Here are some of the properties of seawater activated power batteries.

Table 1. Performance of torpedo powered batteries in various countries [11, 41].

Country	Type	Power/kW	Total weight/kg	Mileage/km
USA	MK45	167	238	10
Italy	A244	30	/	6
Italy	A244/S	32	34	7
UK	Fish	63	57	8
Japan	73 style	54	40	6

2.2.2 Seawater dissolved oxygen batteries

For seawater dissolved oxygen batteries, magnesium is also adopted as the anode while seawater serves as the electrolyte. The difference is that inert electrodes, such as carbon fiber or graphite, are usually used as cathode materials, and oxygen dissolved in seawater is used as oxidant. Oxygen reduction reaction (ORR) takes place on the cathode [42, 43]. Generally, open structure design is adopted for this kind of batteries. The typical structure of a seawater dissolved oxygen battery is depicted in Fig. 3.

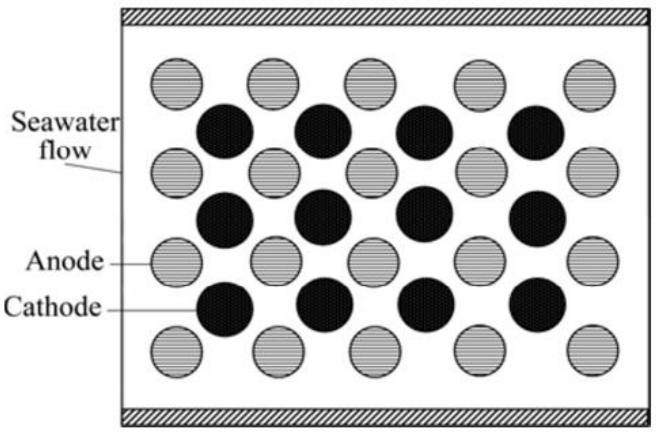

Figure 3. Top view of a seawater dissolved oxygen battery [15].

The electrode and total reactions are as follows:

$$Anode: Mg \rightarrow Mg^{2+} + 2e^{-}$$

$$Cathode: O_2 + 2H_2O + 4e^{-} \rightarrow 4OH^{-}$$

$$Total: 2Mg + O_2 + 2H_2O \rightarrow 2Mg(OH)_2$$

Theoretically, the voltage seawater dissolved oxygen battery could provide is 3.1V [44]. However, the existence of side reaction like self-corrosive hydrogen evolution makes the actual voltage only about 1V. The low concentration of dissolved oxygen in seawater limits the cathode reaction, which leads to a low cathode current and thus low power. As a result, it is usually used for long-term and low-power underwater equipment [22, 45].

Hasvold et al. [46] used four AZ61 alloy rods with a diameter of 18.4 cm and a length of 1.1 m as the anode, and carbon fiber brushes around the magnesium alloy rods as the cathode to develop a long-acting dissolved oxygen battery. At the initial stage, the output voltage of the battery reached 1.2 V. After discharging for 20 h, the voltage stabilized at 1.6-1.7 V. After 635 days of operation, the output voltage began to fluctuate and decreased to a certain extent, providing 55 kilowatt-hours of power at the end. The team [22] later developed an underwater autonomous submersible, which could travel for long distance. It was powered by a magnesium/seawater dissolved oxygen battery, capable of traveling 2963.2 km at a speed of 2 m/s with a power of 133 W.

American Westinghouse company [47] committed to the research of underwater low-power seawater battery for a long time. The team developed a seawater dissolved oxygen battery with catalytically treated carbon/Teflon as the positive electrode material. The battery was a cylindrical structure, capable of providing a stable voltage of 1.3-1.4 V at a power output of 2-3 W, maintaining excellent discharge performance in warm water near the equator and in cold arctic environments.

2.3 Hydrogen peroxide fuel cells

Magnesium/hydrogen peroxide (Mg/H_2O_2) fuel cells use inert electrode with noble metal catalyst loaded onto it as cathode, magnesium as anode while hydrogen peroxide as the cathode active material. A conductive proton exchange membrane is used to separate the anode and cathode [17]. This type of battery has a larger cathodic current density, theoretically, it can provide around 3.25 V voltage even in neutral solution, which is even higher than that of Mg-air battery due to stronger oxidability of H_2O_2. Compared with aluminum anode, there is no need to add additional alkaline electrolyte such as sodium hydroxide for magnesium anode, which can greatly improve its specific energy. The typical structure of one Mg/H_2O_2 fuel cell is depicted in Fig. 4. During the discharge process, the magnesium anode loses electrons, while the hydrogen peroxide gains electrons and is reduced at the inert electrode. Thus the current is generated and the total reaction is established. Here are the electrode and total reactions:

$$Anode: Mg \rightarrow Mg^{2+} + 2e^-$$

$$Cathode: H_2O_2 + 2H^+ + 2e^- \rightarrow 2H_2O$$

$$Total: Mg + H_2O_2 + 2H^+ \rightarrow Mg^{2+} + 2H_2O$$

The above reactions occur in acidic solutions, but in neutral or alkaline cases, the following reactions occur:

$$Anode: Mg \rightarrow Mg^{2+} + 2e^-$$

$$Cathode: HO_2^- + H_2O + 2e^- \rightarrow 3OH^-$$

$$Total: Mg + HO_2^- + H_2O \rightarrow Mg^{2+} + OH^-$$

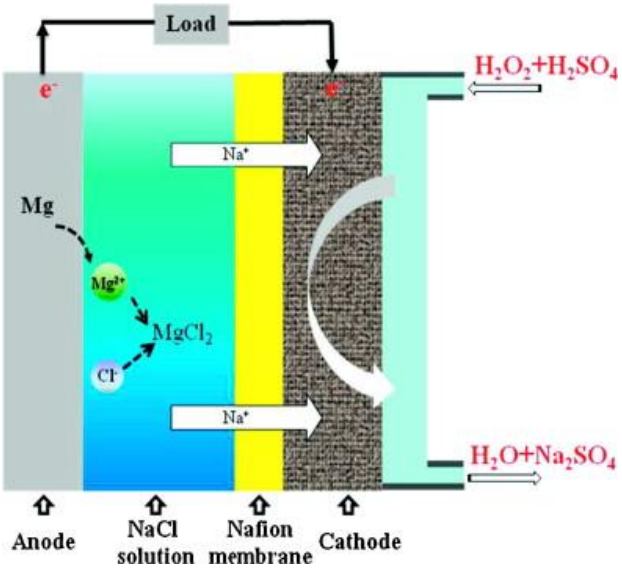

Figure 4. Typical structure of a Mg/H_2O_2 fuel cell in acidic solutions [48].

Hydrogen peroxide fuel cells are usually used in situations where the output power requirement is not too high, such as serving as the power supply for low-speed and long-haul submarines [49].

Hasvold et al. [50] from the Norwegian Defence Research Institute once set out to study a portable aluminum-air semi-fuel cell and successfully applied it to the AUV HUGIN 3000. It could travel up to 60 hours at a speed of 4 nautical miles per hour in the deep sea. Later, a battery pack composed of six such cells in series powered AUV HUGIN 3000. The addition of hydrogen peroxide into the electrolyte is continuous in order that the concentration is kept at a constant while the anode is changed every second or third dive. The energy density could reach100 Wh kg^{-1} based on the total weight of the system [51]. In addition, the team replaced the aluminum anode with magnesium alloy anode to study battery discharge performance, which was expected to provide long-term power for submarine monitoring systems and buoy lights.

Medeiros et al. [52] studied a special magnesium seawater semi-fuel cell (Mg-SFC) system. Magnesium alloy was still adopted as anode while the difference was a solution phase catholyte of hydrogen peroxide (H_2O_2) or hypochlorite in the seawater electrolyte. In this work, a galvanostatic discharge test at 25 mA cm^{-2} for 3600 s was carried out in order to investigate the discharge performance. The voltage was 1.3 V when it adopted such an electrocatalyst of nickel foil catalyzed by noble metals palladium and iridium (Ni-Pd/Ir), while the voltage value increased to 1.5 V with an electrocatalyst of carbon catalyzed by palladium and iridium (C-Pd/Ir). The results showed that the cathode material also played a crucial role in the electrochemical properties of such a SFC system.

Medeiros et al. [53] further studied the Mg/H_2O_2 fuel cell system two years later. They optimized five parameters that influenced the performance of the cell using a taguchi matrix experimental design. The factors included the concentration of hydrogen dioxide catholyte, the flow rates of catholyte and electrolyte (v_1 and v_2), the electrolyte temperature (T) and the applied current density (i), all of which are summarized in Table 2. The optimum conditions for maximum specific energy are shown in Table 3.

Table 2. Test parameters of Mg/H_2O_2 fuel cell.

$[H_2O_2]$ (M)	T (℃)	v_1 ($cm^3\ min^{-1}$)	v_2 ($cm^3\ min^{-1}$)	i ($mA\ cm^{-2}$)
0.20	0.0	25.0	25.0	10.0
0.30	25.0	100.0	100.0	25.0
0.40	50.0	200.0	200.0	50.0

Table 3. Optimum conditions for maximum specific energy.

Parameters	$[H_2O_2]$ (M)	T (℃)	v_1 ($cm^3\ min^{-1}$)	v_2 ($cm^3\ min^{-1}$)	i ($mA\ cm^{-2}$)
Optimum conditions	0.20	25.0	100.0	200.0	25.0

2.4 Primary batteries

Primary batteries are also called galvanic batteries, different from rechargeable batteries, they can be used only once and cannot be recharged. Magnesium primary batteries, usually the magnesium manganese dry cells, adopt magnesium cylinder as the anode and a mixture of manganese dioxide powder, ammonium chloride and carbon black as the cathode. A carbon rod is inserted into the cathode material to act as a conductor for the current. Between the two electrodes is a layer of reinforced isolation paper impregnated with ammonium chloride and magnesium chloride. Magnesium perchlorate serves as the electrolyte. Mg/MnO_2 primary batteries double the battery capacity compared with Zn/MnO_2 batteries [54]. The main advantages of the Mg/MnO_2 batteries over the Zn/MnO_2 ones lie in their higher shelf life, high thermal stability and excellent capacity retention [55].

The typical structure of a Mg/MnO_2 primary battery is depicted in Fig. 5. When discharged, the magnesium anode is quickly activated in the magnesium perchlorate ($Mg(ClO_4)_2$) solution, losing electrons, while the manganese dioxide (MnO_2) receives the circulating electrons and is reduced to manganese oxide at the cathode. The electrode and total reactions are as follows:

$$Anode: Mg + 2OH^- \rightarrow Mg(OH)_2 + 2e^-$$

$$Cathode: 2MnO_2 + H_2O + 2e^- \rightarrow Mn_2O_3 + 2OH^-$$

$$Total: Mg + 2MnO_2 + H_2O \rightarrow Mg(OH)_2 + Mn_2O_3$$

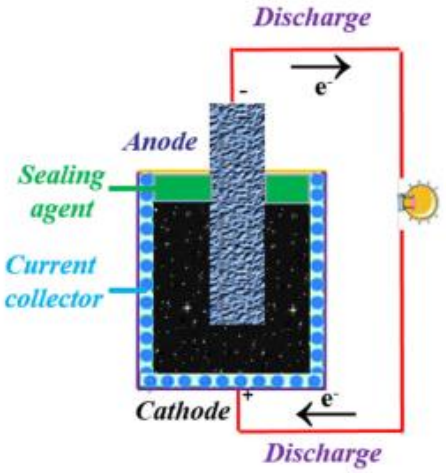

Figure 5. Typical structure of a Mg/MnO_2 primary battery [56].

For a Mg/MnO_2 primary battery, self-corrosion of Mg anode in aqueous solution severely affects its discharge performance and reduces the anode utilization efficiency. Once the battery starts working, the surface of the anode is covered with $Mg(OH)_2$ passivation film, reducing the reaction area and leading to poor discharge performance along with a delayed action that severely restricts the rapid activation. What's worse, the film is unstable and tends to break during the discharge process, so the anode undergoes self-corrosion, resulting in low utilization efficiency.

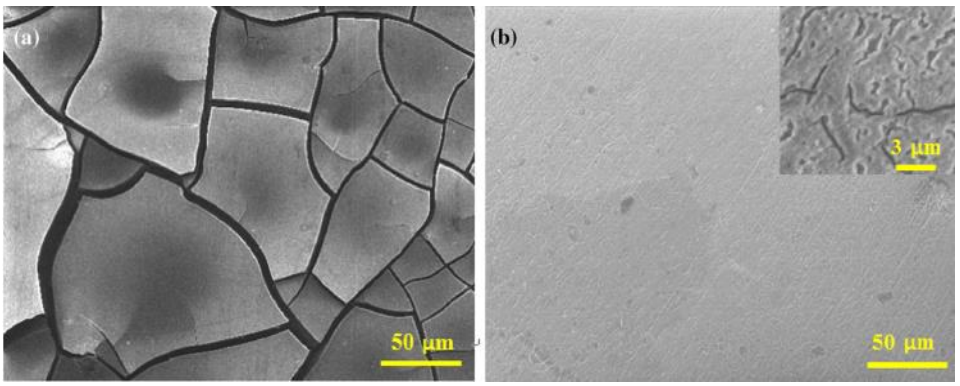

Figure 6. SEM images of magnesium alloy in solution absence (a) and presence (b) NaF-Na_3PO_4 additives after immersion test [56].

Xu et al. [56] explored the influence of fluoride and phosphate additives on the electrochemical behavior of Mg/MnO_2 primary battery. Commercial AZ31B Mg alloy was adopted as anode, the mixture of 85wt% MnO_2 and 15wt% acetylene black served as the cathode in their work. The electrolyte additive amount of NaF and Na_3PO_4 were 30 and 10 mmol L^{-1}, respectively [57]. The addition of NaF-Na_3PO_4 additives improved the performance of Mg/MnO_2 primary battery significantly compared with the one used blank electrolyte. The discharge specific capacity reached 1539 mAh g^{-1} when discharged at the current density of 5 mA cm^{-2}, increasing 37%. The utilization efficiency increased nearly 20%. Fig. 6 illustrated the reason why the corrosion was inhibited. There were obvious cracks on the surface of the

anode (Fig. 6a) while the corrosion film was more compact in NaF-Na_3PO_4 additives electrolyte (Fig. 6b). The magnesium alloy anode was immersed in the electrolyte with NaF-Na_3PO_4 additives for 16 days, but still 95% inhibition efficiency manifested the highly efficient and effective protection of additives to Mg alloys.

Mohanraj [58] prepared a new nano-MnO_2-graphene cathode to enhance the discharge capacity of Mg/MnO_2 primary battery. The cathode material was a mixture of α-MnO_2 nanoparticles and graphene at a mixing ratio of 3:1 by weight with trace amount of polyvinylidene difluoride (PVDF). The discharge performance of the modified Mg/MnO_2 cell was analyzed using galvanostatic discharge tests at the current density of 1, 5, 10 mA cm^{-2}, respectively. The discharge capacity of Mg/MnO_2 primary battery with traditional and modified α-MnO_2 based cathode was summarized in Table 4.

Table 4. Discharge capacity of Mg/MnO_2 primary battery with traditional and modified α-MnO_2 based cathode.

Cathode material	Specific capacity (mAh g^{-1})		
	1 mA cm^{-2}	5 mA cm^{-2}	10 mA cm^{-2}
α-MnO_2	20	46	73
α-MnO_2-graphene	68	308	271

Obviously, the discharge specific capacity of Mg/MnO_2 primary battery based on α-MnO_2-graphene cathode increased many times compared to α-MnO_2 based electrode. This can be attributed to the fact that the manganese dioxide particles were well immobilized on the surface of graphene and well embedded between intermediate layers. With the addition of graphene, the problems of low actual capacity and poor circulability of manganese dioxide were solved, confirming the usefulness of graphene mixed into α-MnO_2 to increase discharge specific capacity of Mg/H_2O_2 primary battery.

2.5 Secondary batteries

The secondary batteries are also known as rechargeable batteries. They refer to the batteries that can return to the initial state and continue to be used by charging after the discharge process. Magnesium secondary batteries, also called as rechargeable magnesium batteries (RMBs), have attracted much attention for its high volumetric energy capacity (3833 mAh cm^{-3}), which is much higher than that of Li-metal batteries [59, 60]. Rechargeable magnesium batteries also adopt magnesium as the anode, but usually the magnesium alloy. For the cathode, some adopt the high-voltage intercalation-type cathode while others apply the high-capacity conversion-type cathode [60]. Transition-metal sulfides and oxides are relatively common cathodes for RMBs. As for the electrolyte, aprotic organic polar solvents are usually taken into consideration [32]. During the discharge process, magnesium loses electrons and cathode active substance gains the electrons while during the charging process, the electrodes react in reverse. The structure of a rechargeable magnesium battery and the electrode reactions are depicted in Fig. 7.

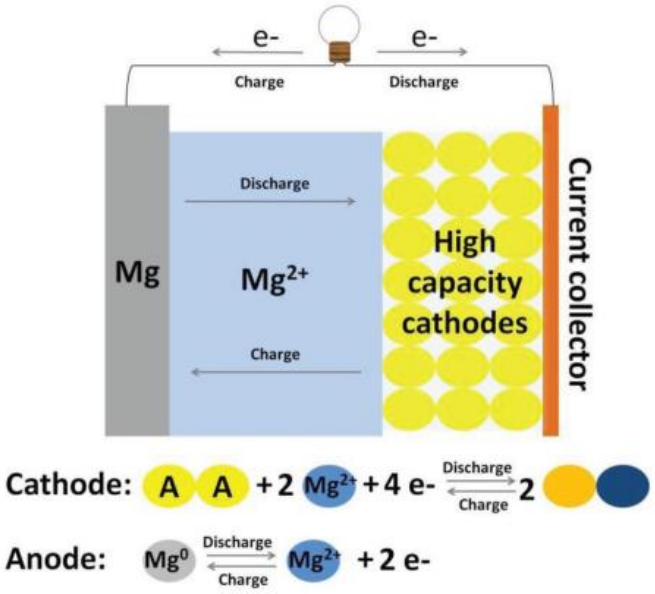

Figure 7. Typical structure of a RMB and the corresponding electrode reactions [60].

As one of the potential strong competitors to replace Li-ion batteries as chemical power supplies in varieties of devices for its lower cost, higher safety, and eco-friendliness [60], the selection of both cathode material and electrolyte also plays a vital role in the electrochemical performance of rechargeable magnesium batteries.

A key technique for developing rechargeable magnesium batteries is to establish a reversible redox process for magnesium. A main difficulty in solving the problem is to modify the electrolytes or develop new and suitable ones that are compatible with the Mg anode and meanwhile promise higher current efficiency and longer cycle life [59]. Magnesium tends to form passivation film in aqueous solution or other protic solvents, making it difficult to establish a reversible redox reaction [61, 62].

A binary ionic liquid (IL) electrolyte which contained organo-magnesium complex was developed by Kakibe et al [63]. The new IL system was based on N,N-diethyl-N-methyl-N-(2-methoxyethyl) anmmonium ($DEME^+$), bis (trifluoromethanesulfonyl) imide ($TFSI^-$) and bis (fluorosulfonyl) imide (FSI^-), written as ($[DEME^+][TFSI^-]_n[FSI^-]_{1-n}$). The chemical structures of the three cations and anions are shown in Fig. 8. The electrochemical behavior of magnesium anode was researched in the new electrolyte system. The cyclic voltammetry results manifested favorable reversibility for the dissolution and deposition of magnesium anode in the new IL electrolyte. In the galvanostatic discharge tests, more than 90% current efficiency can be achieved after charging and discharging for more than 100 laps. Different electrochemical behavior was observed when “n” took different values. The current density for the dissolution of magnesium reached the maximum when n=0.5. Obviously, the mixing ratio of the components played a vital role in the coulombic efficiency. The results also showed that the binary IL system mixed with organo-magnesium complex could serve as promising electrolyte for rechargeable magnesium batteries.

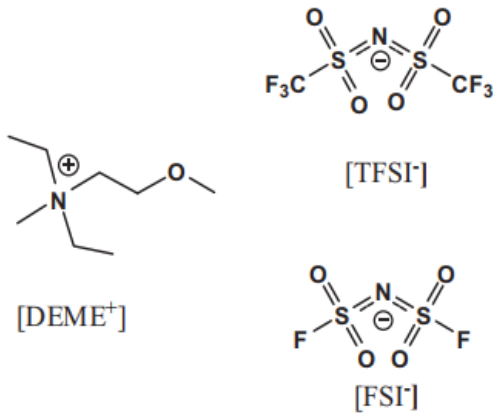

Figure 8. Chemical structures of the ionic liquids.

Another ongoing problem is to develop new cathode materials that allow electrochemical insertion and disembedding of Mg^{2+} ions, which heavily affects the discharge performance of rechargeable magnesium batteries.

Xiao et al. [64] synthesized new-type V_2O_5 microspheres as the cathode for RMBs. The V_2O_5 microspheres exhibited flower-like structure and were synthesized via hydrothermal synthesis method with hexadecyl trimethyl ammonium bromide (HTAB) surfactant. The influence of regular V_2O_5 (r-V_2O_5) microspheres and irregular assembled V_2O_5 (ir-V_2O_5) on electrochemical performance of RMBs was investigated. According to the cyclic voltammetry curves, ir-V_2O_5 presented a similar curve of the first cycles to the r-V_2O_5, but the larger curve area and peak current of r-V_2O_5 suggested that r-V_2O_5 may have a higher capacity. The larger area decrease for ir-V_2O_5 than that of r-V_2O_5 after tenth cycles showed better cycling stability of r-V_2O_5. The rate capability at different current densities also showed that r-V_2O_5 kept higher discharge capacity than ir-V_2O_5. Besides, r-V_2O_5 possessed better reversibility to resist large currents. It can be concluded that r-V_2O_5 displayed better electrochemical performance from the phenomena above, and the values are listed in Table 5.

Table 5. Electrochemical performance and structure parameters of two V_2O_5 particles.

Cathode	Specific capacity (mAh g^{-1}) at 50 mA g^{-1}	Cycling stability (mAh g^{-1}) after 80 cycles	Rate capability (mAh g^{-1}) at 200 mA g^{-1}	Specific surface area (m^2 g^{-1})	Pore volume (cm^3 g^{-1})
ir-V_2O_5	114.3	67.4	30	8.1	0.146
r-V_2O_5	126.2	90.7	60	13.7	0.185

Obviously, structure played a vital role in improving the cathode electrochemical performance of the RMBs according to the results above. The r-V_2O_5 showed larger interspaces and was more stable and flexible than ir-V_2O_5. The morphology images of the two V_2O_5 particles are depicted in Fig. 9. And the nitrogen (N_2) absorption/desorption isotherm of r-V_2O_5 and ir-V_2O_5 further confirmed that the former held larger specific surface area and larger pore volume, the concrete values are also summarized in Table 5. It must be mentioned that hexadecyl trimethyl ammonium bromide (HTAB) was used as the

surfactant to adjust and control the morphology of V_2O_5 cathode in this work. So the importance of surfactant (HTAB) to regulate the structure and morphology of V_2O_5 cathode was also revealed. Redox reaction caused by reversible insertion and disembedding of Mg^{2+} ions at the cathode was the basic principle of RMBs [65] and the total reaction could be written as [66]:

$$xMg^{2+} + V_2O_5 + 2xe^- \leftrightarrow Mg_xV_2O_5$$

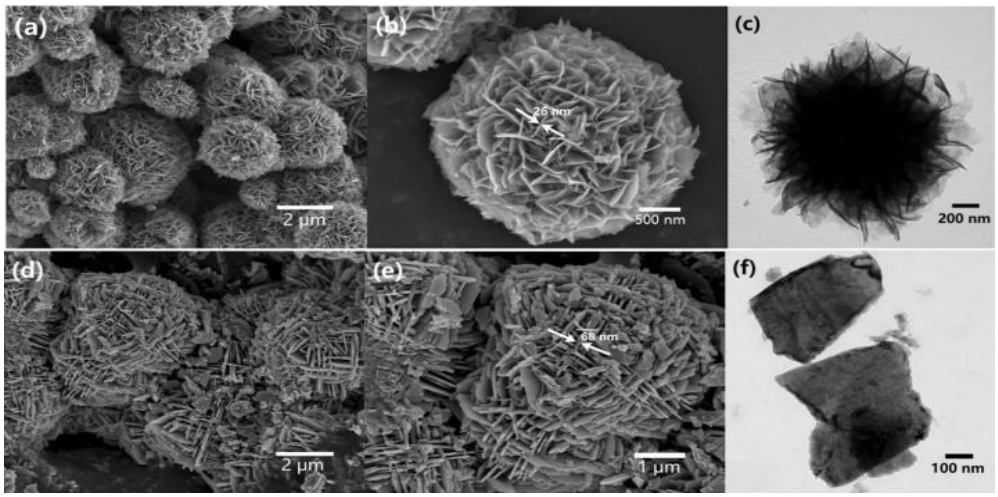

Figure 9. SEM images (a, b, d, e) and TEM images (c, f) of r-V_2O_5 (a–c) and ir-V_2O_5 (d–f) [64].

Another kind of rechargeable magnesium batteries was assembled by Liang and his team [67]. The RMBs took graphene-like MoS_2 (G-MoS_2) as the cathode while nanoscale magnesium (N-Mg) as the anode. In addition, bulk MoS_2 (B-MoS_2) and bulk Mg (B-Mg) were also prepared for comparison. The as-prepared four samples (G-MoS_2, B-MoS_2, N-Mg and B-Mg) were combined in an orthogonal method to study the influence of different active materials on the electrochemical performance separately. Cyclic voltammetry and charge-discharge experiments were carried out to investigate the electrochemical performance of the RMBs. The results are summarized in Table 6.

Table 6. Electrochemical performance of four assembled RMBs.

Types of RMBs	Voltage/V	Specific capacity/mAh g^{-1}	Capacity retention/%
G-MoS_2 / N-Mg	~1.8	170	95%(after 50 circles)
G-MoS_2 / B-Mg	~1.8	85	/
B-MoS_2 / N-Mg	~1.8	71	/
B-MoS_2 / B-Mg	1.64	35	60%(after 5 circles)

As is shown in Table 6, the first three RMBs showed similar operating voltages around 1.8V except the one that used both bulk electrodes. Obviously, B-MoS_2/B-Mg battery provided a lower

operating voltage, which may be ascribed to smaller specific surface area of the bulk electrodes. Even if the operating voltages were the same, the specific capacities of the first three RMBs varied greatly. With the same B-Mg anode, the specific capacity of G-MoS_2/B-Mg battery (85 mAh g^{-1}) is 2.4 times larger than that of B-MoS_2/B-Mg (35 mAh g^{-1}), which maybe lie in easier access of Mg^{2+} ions to the expanded G-MoS_2. G-MoS_2/N-Mg battery exhibited the largest specific capacity, even 4.8 times larger than that of worst-performing B-MoS_2/B-Mg battery. The circulating charge and discharge tests further revealed excellent capacity retention of the G-MoS_2/N-Mg battery and the reactions involved in the process could be established like this:

$$4Mg^{2+} + 6MoS_2 + 8e^- \leftrightarrow Mg_4Mo_6S_{12}$$

The work also demonstrated the importance to regulate the structure and morphology of the electrode materials and provided a direction for the development of high performance RMBs.

3. PROBLEMS AFFECTING MAGNESIUM AS AN ANODE

As mentioned earlier, magnesium can be used as the anode for varieties of batteries, such as Mg-air batteries, seawater batteries, Mg/H_2O_2 fuel cells, primary batteries and rechargeable magnesium batteries due to its inherent advantages like negative electrode potential (-2.37 V vs. SHE), high theoretical specific capacity (2205 mAh g^{-1}) and high energy density (3910 Wh kg^{-1}) [6-11, 67], along with low density (1.74 g cm^{-3}), great raw material abundance and environmental friendliness [12, 67]. However, there also exist some problems adversely limiting the widespread use of magnesium as an anode material.

Firstly, $Mg(OH)_2$ passivation film tends to form on the surface of magnesium when the electrode comes into contact with a reductive substance such as oxygen, water and other aqueous electrolytes [68]. The film is truly passivating and covers the surface of the magnesium electrode, reducing the reaction area. Concomitant irreversible polarization brings about the problems that the electrode activity decreases and the discharge potential shifts positively [69], severely affecting its electrochemical performance as an anode.

Secondly, magnesium suffers drastic self-corrosion in the process of discharge. The corrosion reaction can be written as follows [6]:

$$Mg \rightarrow Mg^{2+} + 2e^- \quad (anodic\ reaction)$$
$$2H_2O + 2e^- \rightarrow H_2 + 2OH^- \quad (cathodic\ reaction)$$
$$Mg^{2+} + 2OH^- \rightarrow Mg(OH)_2 \quad (product\ formation)$$
$$Mg + 2H_2O \rightarrow Mg(OH)_2 + H_2 \quad (over\ corrosion\ reaction)$$

The involved cathodic reaction is the so-called hydrogen evolution reaction (HER), which results in more severe corrosion of magnesium. Galvanic corrosion is another form of self-corrosion and inevitably occurs due to the presence of impurities or second phases. The driving force comes from the electrode potential difference between two different metals or different phases in contact. The corrosion accelerates for those showing more negative potential, while the metal or phase possessing more positive

potential is protected. Obviously, the corrosion of magnesium is accelerated due to its highly negative electrode potential as an anode. Magnesium is not totally used in the electrochemical discharge process for current generation due to the self-corrosion, leading to a low utilization efficiency and actual specific capacity [6, 15].

Thirdly, negative difference effect (NDE) also accelerates the corrosion of magnesium. NDE is a phenomenon in which both cathodic and anodic current increase with the imposed voltage, which is quite different from that of iron, zinc or steel. For most metals, the anodic current rises while the cathodic current decreases simultaneously with the increasing potential. Obviously, the NDE accelerates the hydrogen evolution reaction and thus results in more severe corrosion of magnesium [6].

As discussed above, $Mg(OH)_2$ passivation film, severe self-corrosion and low utilization efficiency are three main problems remaining to be solved yet [6, 15, 68, 69]. The dense passivation film should be removed to expose more contact area while self-corrosion and hydrogen evolution should be restricted to the utmost for a high utilization efficiency. In fact, current research on magnesium anodes has always been focusing on landing a balance between activation and passivation of magnesium. Therefore, it is of significant importance to develop an ideal magnesium anode with both high discharge activity and high anodic utilization efficiency [56].

4. METHODS TO ENHANCE ELECTROCHEMICAL PROPERTIES OF MAGNESIUM ANODE

An ideal magnesium anode should be characterized by both high discharge activity and high utilization efficiency and minimize the rate of self-corrosion. So far, varieties of methods have been used to improve the electrochemical properties and corrosion resistance of magnesium anodes. The most commonly used methods include alloying, heat treatment, plastic deformation and electrolyte modification. In recent years, the first-principle calculations have attracted increasing attention and have been applied to predict the performance of magnesium anodes and explain the corresponding reasons with the development of quantum chemical theory. The theoretical results usually agree well with the experimental results and point out the experimental direction. The methods mentioned earlier are elaborated below.

4.1 Alloying

Alloying is the most widely used and effective method to improve the performance of magnesium anodes. The selection of alloying elements is of great significance and has vital influence on the electrochemical and corrosion performance of the anode. They should either promote the exfoliation of discharge products, or promote the dissolution and redeposition of magnesium, or reduce the solubility of impurity elements. Generally they have a high hydrogen evolution over-potential [15]. Common elements such as Al, Zn, Sn, Pb, Ga, In and RE have been used for alloying. Magnesium anodes doped with different elements are summarized below and grouped into different series.

4.1.1 Mg-Al-Pb series alloys

Aluminum (Al) and lead (Pb) have always been used as the main elements in magnesium alloying as reported in previous investigations [70-73], and the performance of magnesium anode is usually improved by synergies between aluminum and lead.

Li et al. [74] investigated the electrochemical performance of Mg-Al-Pb-(Zn) series alloys as the anodes for seawater activated batteries through an orthogonal array (OA) and then the corresponding signal-to-noise (S/N) ratios were calculated to determine suitable composition for better electrochemical performance. Based on the S/N ratio results of corrosion current density (i_{corr}), average discharge potential (E_{AVG}) and charge transfer resistance (R_t), an optimal magnesium alloy anode Mg-6%Al-7%Pb-0.5%Zn was prepared. Aluminium primarily influenced the i_{corr}, R_t and E_{AVG} at 150 mA cm^{-2}, whereas lead had predominant influence on the electrochemical performance when discharged at 350 mA cm^{-2}. Subsequently, another group of galvanostatic measurements of the as-prepared alloy were carried out at 150 and 350 mA cm^{-2} with commercial AZ31 magnesium alloy as contrast. The results obviously showed that the as-prepared Mg-6%Al-7%Pb-0.5%Zn alloy provided much more negative average discharge potentials than commercial AZ31 alloy when discharged at both 150 and 350 mA cm^{-2}, as is summarized in Table 7. Besides, the Mg-6%Al-7%Pb-0.5%Zn alloy exhibited higher anodic utilization efficiencies at both 150 and 350 mA cm^{-2}, reaching 87.4% and 86.1%, respectively. The assembled battery with the electrodes of as-prepared Mg-6%Al-7%Pb-0.5%Zn alloy and AgCl obtained an excellent specific energy of 155 Wh kg^{-1}.

New Mg_2Pb phase was found in the as-prepared alloy, which showed more fine grains, facilitating the peeling of hydroxide film. The better discharge properties could be ascribed to the recrystallization and more corrosion sites such as the surroundings of new Mg_2Pb phase, which served as a cathode phase towards the α-Mg matrix.

Table 7. Average discharge potential of Mg-6%Al-7%Pb-0.5%Zn and AZ31 alloys [74].

Mg anodes	Average discharge potential (V) (vs. SCE)	
	150 mA cm^{-2}	350 mA cm^{-2}
AZ31	-1.0928	-0.7972
Mg-6%Al-7%Pb-0.5%Zn	-1.6772	-1.3491

Feng et al. [75] investigated the influence of cerium (Ce) addition to Mg-Al-Pb series alloys for the increase of anodic efficiency. A new Mg-6%Al-5%Pb-0.6%Ce alloy anode was prepared and the Mg-6%Al-5%Pb alloy without Ce addition was used as a contrast. Subsequently, a series of electrochemical measurements and morphology characterization were carried out. Differences in polarization curves indicated different electrode reactions. Cathodic branches of the two alloys showed totally different trends, certifying that the addition of Ce changed the hydrogen evolution reaction (HER) of Mg-Al-Pb alloy. Besides, the anodic tafel slope of Mg-Al-Pb-Ce alloy decreased with the addition of Ce compared with Mg-Al-Pb alloy, which may be attributed to the improved anodic dissolution activity

caused by Ce. The addition of Ce negatively shifted the average discharge potential by about 100 mV in this study. According to the microstructure analyses, the second phase γ-$Al_{11}Ce_3$ and β-$Mg_{17}Al_{12}$ were found dispersively distributed in Mg-Al-Pb-Ce alloy. The addition of Ce distinctly refined the grains and promoted the formation of new γ-$Al_{11}Ce_3$ second phase, which not only acted as a weak cathode phase but also led to the uniform distribution of β-$Mg_{17}Al_{12}$ second phase in the magnesium matrix, thus the Mg-Al-Pb-Ce alloy showed better discharge activity. The average discharge potential and utilization efficiency were summarized in Table 8.

Table 8. Average discharge potential and utilization efficiency of Mg-Al-Pb-Ce and Mg-Al-Pb alloys.

Mg anodes	Average discharge potential (V) (vs. SCE)	Utilization efficiency η/%
	180 mA cm^{-2} for 600 s	180 mA cm^{-2} for 1 h
Mg−6%Al−5%Pb	-1.648	67.7±0.2
Mg−6%Al−5%Pb−0.6%Ce	-1.756	74.7±0.4

Wang et al. [76] investigated the influence of Al and Pb addition on the corrosion performance of magnesium anode. An activation mechanism of dissolution-reprecipitation was proposed to explain the reason why the discharge activity was improved. In this work, an interesting phenomenon was found that the influence of Pb on the corrosion behavior depended largely on the content of Al. The corrosion rate of Mg-Al-Pb alloy decreased with the increasing Al content. Only when the content of Al is low, Pb addition also decreased the corrosion rate. In the potentiodynamic polarization measurements, the anodic current of the prepared Mg-9%Al-2.5%Pb increased heavily with the increasing imposed potential during anodic dissolution, meaning the best discharge activity. The optimal Mg-9%Al-2.5%Pb alloy reached an average discharge potential of -1.598V (vs. SCE) and a high anode utilization efficiency of 79.2%. The second phase β-$Mg_{17}Al_{12}$ was still found in the Mg-9%Al-2.5%Pb alloy and the volume fraction of β-$Mg_{17}Al_{12}$ increased with increasing Al content. As a result, the corrosion rate of Mg-Al-Pb alloy decreased due to the barrier effect rather than the galvanic corrosion effect of second phase, which was consistent with early results [77, 78]. A dissolution-reprecipitation mechanism for activation indicated that the precipitation of Pb^{2+} ions destroyed the $Mg(OH)_2$ passivation film, while the precipitation of Al^{3+} ions synergistically promoted the peeling of $Mg(OH)_2$ further.

4.1.2 Mg-Al-Sn series alloys

Mg-Al-Pb series alloys have been developed to be used as the anodes for seawater activated batteries as mentioned earlier [74-76] due to the achieved high discharge activity. However, the addition of poisonous element Pb also brought about some problems so that they had not been widely used as commercial anode materials for chemical power supplies yet. To replace the poisonous element Pb, Mg-

Al-Sn series alloys were developed to promise both excellent discharge activity and satisfactory utilization efficiency.

Yu et al. [79] developed a new Mg-6%Al-1%Sn (AS61) alloy, and a higher Sn content of Mg-6%Al-5%Sn (AS65) alloy was used as a contrast. The electrochemical properties of the prepared Mg-Al-Sn alloys were compared with that of commercial AZ31 and AP65 alloys. The galvanostatic discharge results under 100 mA cm^{-2} showed that AS61 alloy possessed more negative average discharge potential of -1.611 V than the other three alloys and thus the best discharge activity. A dispersed ternary $Mg_{17}(Al,Sn)_{12}$ phase was found uniformly distributed around the Mg matrix, which served as a cathode phase promoting the corrosion of Mg matrix, improving the discharge activity. However, another second phase Mg_2Sn was found in AS65 alloy with the increase of Sn content, which showed a larger size and distributed inhomogeneously around the α-Mg matrix. Obviously, the existence of $Mg_{17}(Al,Sn)_{12}$ phase improved the discharge activity, whose dispersed distribution promised more uniform electrochemical dissolution and let more electrolyte penetrate into the interior of the anode through the cracks on the surface, accounting for better discharge activity of AS61 than AS65.

4.1.3 Mg-Al-Zn series alloys

Li et al. [80] developed a series of Mg-Al-Zn alloys and investigated the effect of indium (In) on the electrochemical performance. In the galvanostatic discharge tests, the imposed current density ranged from 10 to 200 mA cm^{-2}, aiming to research the discharge behavior of magnesium alloy anodes under different conditions. The prepared Mg-6%Al-3%Zn-1%In (AZ63-1%In) always exhibited the most negative average discharge potential while the anodic efficiency was slightly lower than that of Mg-6%Al-3%Zn-2%In (AZ63-2%In) when applied larger current densities. Obviously, the addition of In increased the electrochemical activity of the AZ63 alloy. Taking both corrosion resistance and electrochemical activity into consideration, the optimum amount of In addition was 1.0%. In the structure characterization, discontinuous β-$Mg_{17}Al_{12}$ phases were found along the grain boundaries with α-Mg surrounded by eutectic α, which served as a barrier to slow down the corrosion. It could be inferred that In favored the segregation from the matrix and separated the precipitation in α-Mg or the eutectic α phase from the SEM-EDS results. Adding the right amount of In promoted the self-exfoliation of the discharge product and promised better discharge activity. The involved dissolving-reprecipitation mechanism caused by In addition could be written as:

$$M(In) \rightarrow M^{n+} + In^{3+} + (n+3)e^-$$
$$M + In^{3+} \rightarrow M^{n+} + In + (n-3)e^-$$

which promoted the dissolution of magnesium and thus showed higher discharge activity.

Zhao et al. [81] investigated the electrochemical properties of Mg-9%Al-x%Zn series alloys with different zinc content. The influence caused by different zinc content on Mg-Al series alloys was investigated. Among the three prepared alloys Mg-9%Al-0.5%Zn, Mg-9%Al-0.7%Zn and Mg-9%Al-1.0%Zn, Mg-9%Al-1.0%Zn alloy exhibited the best corrosion resistance according to the potentiodynamic polarization curves, and the corrosion resistance improved with the increase of zinc content. The utilization efficiency results were in excellent accordance with the corrosion resistance. It

could be concluded that the addition of zinc contributed to the enhancement of the corrosion resistance and anodic utilization efficiency. Dramatically, good discharge activity was not simultaneously obtained, meaning a new task to achieve the balance of activation and passivation.

4.1.4 Mg-RE series alloys

In addition to common elements, rare earth (RE) elements also play a significant role in the improvement of magnesium anode performance. A large number of studies have shown that RE could improve the corrosion resistance and discharge activity of magnesium anodes greatly [82, 83].

Feng et al. [84] investigated the effects of rare earth elements cerium (Ce) and yttrium (Y) on the electrochemical behavior of magnesium alloy at small current densities. The polarization curve tests showed that multi-element Mg-Al-Pb-Ce-Y alloy exhibited much more negative discharge potential than Mg-Al-Pb alloy. Minor Ce and Y negatively shifted the corrosion potential of the Mg-Al-Pb alloy. The current density increased rapidly with increasing potential in anodic branch, indicating strong discharge activity. Mg-Al-Pb-Ce-Y alloy with minor Ce and Y addition was found to exhibit finer dendrite crystals. A new γ phase, which was the gathering of Al_2Ce and Al_2Y particles, distributed uniformly in the α-Mg matrix. This new γ phase modified the morphology of the β-$Mg_{17}Al_{12}$, which served as the cathode phase to accelerate the galvanic corrosion of α-Mg matrix due to its small volume fraction. Besides, the new dispersed γ phase possessed more negative electrode potential than that of the β-$Mg_{17}Al_{12}$ phase, reducing the potential difference between the second phase and the matrix. The galvanic corrosion of Mg-Al-Pb-Ce-Y alloy was restricted so this anode showed better corrosion resistance due to the weak cathodic effect of γ phase.

Wang et al. [85] developed a Mg-Li-Al-Ce-Y-Zn alloy anode with the discharge performance and corrosion behavior investigated. According to the galvanostatic discharge tests, the anode utilization efficiency of the prepared Mg-Li-Al-Ce-Y-Zn anode reached around 60.6% when discharged at a small current density, which was even higher than that of the commercial AP65 alloy. Based on the phase analyses, a new AlLi phase was detected only in Mg-Li-Al-Ce-Y-Zn alloy anode while not found in Mg-Li-Al-Ce-Y alloy. Zinc mainly distributed in the β-Li phase of Mg-Li-Al-Ce-Y-Zn alloy and this metal possessed more positive standard electrode potential than magnesium and lithium, reducing the electrode potential difference between α-Mg and β-Li phases. Therefore, Mg-Li-Al-Ce-Y-Zn alloy exhibited weak micro-galvanic corrosion. Besides, zinc promoted the formation of AlLi particles, which served as the active sites and accelerated the spalling of the discharge products, improving the discharge activity. Zinc in Mg-Li-Al-Ce-Y-Zn alloy favored the uniform dissolution of the anode, avoiding the severe detachment of α-Mg matrix. Thus, Mg-Li-Al-Ce-Y-Zn alloy showed higher utilization efficiency. For subsequently assembled Mg-air battery, a peak power density of 92.25 mW cm^{-2} was achieved, which was even comparable with that of a Mg/H_2O_2 fuel cell.

Ma et al. [7] developed a Mg-14%Li-1%Al-0.1%Ce alloy. Its electrochemical performance as the anode for Mg-air battery was investigated with pure Mg and commercial AZ31 alloy as a contrast. The newly-prepared alloy exhibited the lowest corrosion rate but the best discharge activity at the same time. Small current densities with the range from 0.5 to 10 mA cm^{-2} were imposed in the galvanostatic

discharge tests for long-duration and low-power batteries. This alloy showed higher operating voltage and anode utilization efficiency than that of pure Mg and AZ31 alloy at all current densities. The best electrochemical properties of the assembled Mg-air battery with the new anode were achieved when discharged at 2.5 mA cm^{-2} with an anode utilization efficiency of 85.2% and a specific capacity of 2072 mAh g^{-1}. Obviously, the anode was suitable for small current discharge and for low-power applications [86]. As for the discharge product film, it was loose and porous and had many cracks, allowing the electrolyte to penetrate through and obtaining larger contact area during discharge, which accounted for its high discharge activity.

4.2 Heat treatment

While alloying is used to improve the corrosion resistance and electrochemical performance of magnesium alloys, heat treatment is another effective method to improve the anode performance further and is also widely studied. The combination of alloying and subsequent heat treatment is of great significance and really works, which has attracted extensive attention. Heat treatment could change the microstructure and favors the compositional homogeneity of magnesium alloys, thus improves the discharge activity [15, 87-90]. Besides, heat treatment usually changes the number and distribution of second phases around the magnesium matrix, which serve as the local cathodes and trigger more severe galvanic corrosion in most cases. Common heat treatment methods to improve the properties of magnesium alloys include homogenized annealing treatment (T2), solid solution treatment (T4), aging treatment (T5), solid solution and subsequent stabilization treatment (T7) and annealing after plastic deformation and so on [15].

Wang et al. [87] developed a series of Mg-9%Al-2.5%Pb alloys and studied the influence of solution and aging treatments on its electrochemical performance in artificial seawater. The results suggested that the discharge activity of the prepared Mg-9%Al-2.5%Pb alloy decreased but the anodic efficiency slightly increased after only solution treatment. However, both discharge activity and utilization efficiency were enhanced after aging at 200℃ for 12 h. The alloy that underwent solution and subsequent aging treatment exhibited the best discharge activity and kept a stable potential during the middle and late stage of discharge among the four alloy samples. Besides, the anodic utilization efficiency reached about 84%. More electrolyte penetrated into the inner alloy and boosted the self-exfoliation of the discharge products due to their loose and uneven structures, which may account for the good discharge behavior of the treated alloy. The alloys were treated at different temperatures and the results indicated that the aging temperature also had a great influence on aging treatment and consequently the anode properties.

Xiong et al. [88] reported a method of hot extrusion and subsequent annealing treatment to enhance the electrochemical performance of Mg-6%Al-1%Sn alloy. The annealing process was performed at 200℃ and the treated Mg-Al-Sn alloy exhibited more negative discharge potential and higher anodic utilization efficiency than other alloys. It was also worth mentioning that the phenomenon was more obvious at a larger current density, with the utilization efficiency even twice as much as that at small current density. A Mg-air battery was then assembled with the annealed Mg-Al-Sn alloy as the

anode, promising a high peak power density of 94.1 mW cm^{-2}, which is comparable with that of Mg/H_2O_2 fuel cell that used Mg-Li based alloy as the anode [89].

The microstructure of the hot-extruded alloy was non-uniform, while it was fully refined after subsequent 200℃ annealing treatment. It can be learned that the annealing treatment promoted the precipitation of the second phase and another spherical Mg_2Sn phase, which homogeneously distributed in the Mg-Al-Sn alloy. The recrystallized microstructure accelerated the self-exfoliation of corrosion products, leading to a high discharge activity. Optical microscopy images of the alloys in four different states were shown in Fig.10. Obviously, homogenization treatment contributed to the dissolution of plenty of second phases into the matrix and the increase of grain size. It could be also shown that hot extrusion promoted the grain refinement of the homogenized alloy while fully recrystallized and uniform microstructure was obtained after the 200℃ annealing treatment.

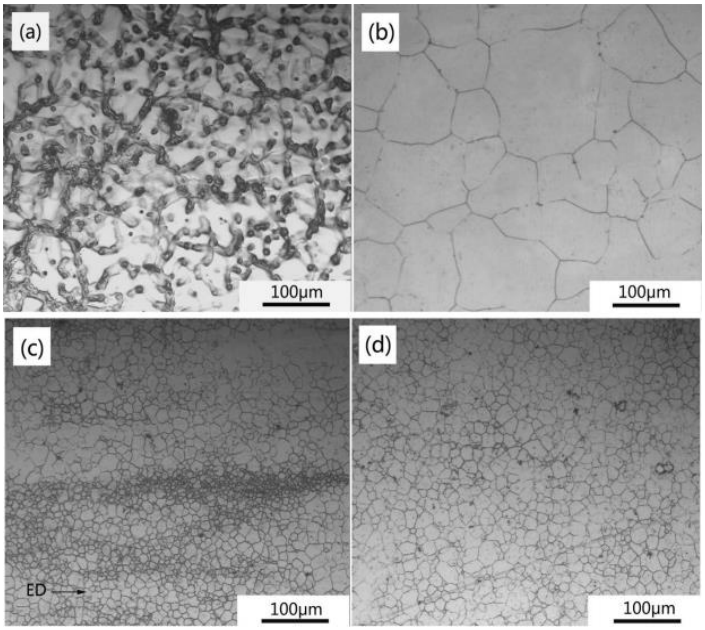

Figure 10. Optical microscopy images of Mg-Al-Sn alloys under different states. (a) as-cast alloy, (b) homogenization treatment, (c) extrusion treatment, (d) annealing treatment [88].

Heat treatment is often accompanied by the process of plastic deformation [15], as mentioned in ref [88]. Hot extrusion was carried out before annealing treatment. Similarly, Wang et al. [71] investigated the influence of hot rolling and subsequent annealing treatment on the electrochemical performance of AP65 alloy anode. In this study, AP65 alloy was processed by hot rolling with many passes and the subsequent annealing treatment at 150 and 350℃, respectively. AP65 magnesium alloys under different states were studied, with pure Mg and commercial AZ31 alloy as a contrast. The results of potentiodynamic polarization showed that the 150 ℃ annealed alloy exhibited better discharge activity at both the corrosion potential and the condition of anodic polarization. The imposed current densities were 10 and 180 mA cm^{-2} in the galvanostatic discharge process, with the low current density

evaluating the discharge behavior for long-duration and low-power applications while the high current density for high-power devices [13]. The 150℃ annealed AP65 alloy exhibited the most negative discharge potential at both 10 and 180 mA cm^{-2}, reaching -1.780 V and -1.686 V, respectively. The explanation for this may focus on the microstructure. β-$Mg_{17}Al_{12}$ phase as a barrier [90, 91] in the as-cast AP65 alloy hindered the galvanic corrosion process, and the homogenized alloy after annealing possessed stronger discharge activity than the as-cast ones. It could be ascribed to the existence of β-$Mg_{17}Al_{12}$ phase and the formation of the Al-Mn particles, which served as strong cathode phases to accelerate the discharge process. Hot rolling process refined the grains and the subsequent annealing at 150℃ reduced the high density of dislocations, as is known, the abundant dislocations possess high deformation energy, which is unfavorable to the anode properties [92, 93]. The study also revealed that annealing should be kept at a proper temperature like 150℃ rather than a higher 350℃.

4.3 Plastic deformation

Plastic deformation is another effective method to improve the electrochemical properties of magnesium alloys, which could modify the microstructure distinctly. Poor deformability of magnesium due to the hexagonal close packed (HCP) structure limits its direct application as anode materials. Consequently, magnesium alloys are mostly subjected to hot rolling or hot extrusion to eliminate stress [15]. Plastic deformation usually results in the change of grain orientation, which in turn affects the electrochemical properties of magnesium alloys obviously [90, 94]. There have been many studies on the plastic deformation for the enhancement of electrochemical performance of magnesium alloys.

Shi et al. [95] reported the effect of hot extrusion on the discharge properties for Mg-Al-Pb anode doped with rare earth element lanthanum (La). In this work, the as-cast alloys underwent solution treatment, water quenching and final hot extrusion treatment successively. The study highlighted different microstructure and the corresponding performance between transverse sections along the radial direction (RD) and longitudinal sections along the extrusion direction (ED), as is shown in Fig. 11. For the extruded alloys, Mg-Al-Pb-La alloy showed increased grain sizes than the ones without La addition, which led to less grain boundaries of the extruded Mg-Al-Pb-La than the Mg-Al-Pb alloy. The polarization curves results indicated that the extruded Mg-Al-Pb-La exhibited more negative corrosion potential (E_{corr}), meaning a stronger discharge activity [74, 96], but a smaller corrosion current density (i_{corr}) signified increased corrosion resistance [97]. According to the galvanostatic discharge results, the average discharge potential of the extruded Mg-Al-Pb-La along ED even reached -1.761V, and the anodic efficiency nearly 90%. The peak power density of an assembled battery with CuCl as the cathode reached 260.8 mW cm^{-2} when discharged at 300 mA cm^{-2}, which was even higher than that of a Mg/H_2O_2 fuel cell. Obviously, the alloy after hot extrusion showed better discharge activity and higher anodic efficiency, which could be attributed to 1) the formation of evenly-distributed β-$Al_{11}La_3$ phase and promoted recrystallization by lanthanum addition, 2) less dislocations and twin defects after hot extrusion.

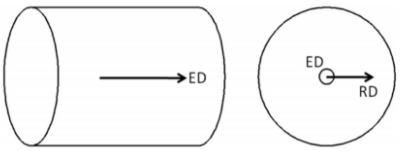

Figure 11. Sampling directions (longitudinal sections and transverse sections).

Similar research was also carried out by Wang et al. [72]. The team reported the enhanced discharge activity of AP65 alloy by hot extrusion, meeting the needs of an anode used for high-power system. AP65 alloy after hot extrusion exhibited larger corrosion current density and was quickly activated in the discharge process. In the study, a small current density was imposed to research the discharge performance for low-power system while larger current densities for high-power devices [13, 71]. The extruded AP65 showed more negative average discharge potentials than the non-extruded ones at all current densities. It was also worth mentioning that the activation time [98] was significantly shortened after extrusion treatment, which could be ascribed to its favourable microstructure and better compositional homogeneity of the matrix aroused by extrusion process. Besides, the refined grains (Fig.12), lower dislocation density and cracked Al_8Mn_5 phase after extrusion improved the corrosion resistance of AP65 alloy and thus a promising utilization efficiency especially at larger current density, meaning the alloy was more suitable for high-power battery system. But plenty of metallic pieces were detached when discharged at small current density, leading to a low anodic efficiency.

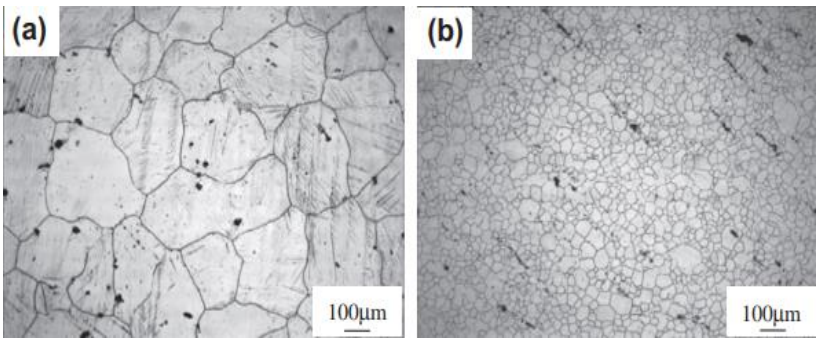

Figure 12. Optical microscopy images of extruded AP65 (a) and non-extruded AP65 (b) [72].

In addition to hot extrusion, hot rolling can also bring a great impact on the discharge activity and corrosion behavior of magnesium alloys. Wang et al. [99] investigated the discharge performance and corrosion properties of AP65 alloy with different rolling reductions. A multi-pass rolling method was adopted in this study, aiming to find the optimum rolling reduction to improve the properties of AP65 as anodes. The as-cast alloy underwent homogenization and multi-pass rolling with different rolling reductions of 0%, 38%, 63% and 86%, respectively. The results of electrochemical tests showed that the rolling with 63% reduction improved the properties most significantly. 63% deformation uniformly refined the grains and the Al_8Mn_5 particles were fractured, and more nanometer sub-grains were found to distribute homogeneously in the matrix. Consequently, the alloy exhibited enhanced

electrochemical activity and corrosion resistance with a high anodic efficiency of nearly 88.9% at 180 mA cm^{-2}. It could also be learned that higher rolling reduction of 86% further boosted the recrystallization, but more defects and dislocations were also produced at the same time, adversely affecting the anode performance of AP65 alloy on the contrary.

Apart from the aforementionedAP65 alloy, hot rolling is also applied for Mg-Hg-Ga series alloy. Wu et al. [100] developed a new Mg-1.6%Hg-2%Ga alloy and investigated the influence of hot rolling on its electrochemical behavior. The as-cast Mg-1.6%Hg-2%Ga alloy underwent homogenization, hot extrusion and multi-pass hot rolling process successively. The results of electrochemical tests showed a dramatic phenomenon where the prepared hot-rolled alloy with a final thickness of 0.35 mm possessed weakened discharged activity but quite high anodic efficiency. The hot rolling treatment even increased the utilization efficiency to unbelievable 87.16% even at a small current density of 20 mA cm^{-2}. However, this went against the goal of improving the properties of magnesium alloys as anodes because the utilization efficiency was significantly increased while the discharge activity was slightly weakened. Hot rolling refined the grains and facilitated the precipitation of Mg_5Ga_2 and $Mg_{21}Ga_5Hg_3$ particles, with nearly no magnesium matrix detached. Considering both the average discharge potential and the utilization efficiency in Table 9, it can be concluded that the rolled Mg-Hg-Ga alloy was more suitable for low-power equipment rather than high-power ones.

Table 9. Average discharge potential and the utilization efficiency of Mg-Hg-Ga alloys discharged at 180 and 20 mA cm^{-2}.

Sample	E_{mean} (vs. SCE)/ V		Utilization efficiency, η/ %	
	180 mA cm^{-2}	20 mA cm^{-2}	180 mA cm^{-2}	20 mA cm^{-2}
0.35mm	-1.557	-1.772	88.94	87.16
0.80mm	-1.733	-1.866	63.75	42.72
Extruded	-1.722	-1.912	54.47	38.90
Homogenized	-1.897	-1.979	74.12	24.60
As-cast	-1.775	-1.960	63.94	27.98

4.4 Electrolyte modification and optimization

In addition to the researches that enhance the anode performance directly, there are not a few studies aimed at electrolyte modification for improving the electrochemical performance of magnesium alloys. It has always been considered as a convenient but effective way to add additives to the electrolyte [15, 17, 101, 102], which could be ascribed that: 1) the electrolyte affects the transfer and diffusion of protons and other aggressive ions, 2) the electrolyte affects the dissolution of magnesium, 3) the electrolyte affects the formation and exfoliation of $Mg(OH)_2$ passivation film even its compactness [15]. These signify that the electrochemical properties of magnesium alloy could be enhanced by electrolyte modification and optimization.

Cao et al. [17] researched the influence of gallium oxide (Ga_2O_3) addition on the electrochemical performance of different magnesium alloys like Mg-Li, Mg-Li-Al and Mg-Li-Al-Ce. In the work, obvious difference for the anodic utilization efficiency was observed after 0.05 mM Ga_2O_3 was added into the electrolyte. Firstly, alloying affected the electrochemical properties of the alloy, the discharge activity and anodic utilization efficiency of these alloys increased in the order: Mg-Li< Mg-Li-Al< Mg-Li-Al-Ce. Secondly, based on the best-performed Mg-Li-Al-Ce alloy, trace amount of Ga_2O_3 was added into the electrolyte and improved both the electrochemical activity and anodic efficiency. There existed 6% increase in the anodic utilization efficiency. Obviously, Ga_2O_3 could serve as an effective additive applied to the electrolyte. The microstructure analyses also indicated that the addition of Ga_2O_3 loosened the product film $Mg(OH)_2$ and promoted its self-peeling from the electrode surface, leading to more contact of the alloy anode to the electrolyte and thus improved the discharge behavior of the magnesium alloy.

Li et al. [101] investigated the effect of the addition of sodium phosphate (Na_3PO_4) and sodium dodecylbenzenesulfonate (SDBS) on the electrochemical behavior of commercial AZ91 alloy. In this study, the electrochemical and corrosion behavior of AZ91 in four different electrolytes (Table 10) were tested. Based on the corrosion rate (v), the inhibition efficiency (IE) was innovatively proposed to describe the self-corrosion. The inhibition efficiency (IE) could be expressed as:

$$IE = \frac{v - v_0}{v} \times 100\%$$

whereas v means the corrosion rate ($g\,cm^{-2}\,h^{-1}$) of the alloy anodes soaked in electrolyte without additives, and v_0 denotes the corrosion rate of those soaked in the electrolyte with different additives. The experiment demonstrated that the corrosion rate of AZ91 alloy was greatly decreased after the addition of 0.05 g L^{-1} Na_3PO_4 and 0.05 g L^{-1} SDBS mixture. The inhibition efficiency of d) electrolyte reached as high as 95.2%. And the assembled battery with d) electrolyte exhibited more negative discharge potential and higher anodic efficiency, which could be ascribed to the accumulation decrease of discharge product and the formation of more cracks on the surface of the anode.

Table 10. Composition of four different electrolytes used in the work.

Electrolyte	Composition
a)	3.5%NaCl (blank control)
b)	3.5%NaCl+ 0.05gL^{-1} Na_3PO_4
c)	3.5%NaCl+0.05gL^{-1} SDBS
d)	3.5%NaCl+0.05 g L^{-1} Na_3PO_4+0.05 g L^{-1}SDBS

Lv et al. [102] investigated the influence of sodium fluoride (NaF) on the electrochemical properties of the multi-element Mg-11%Li-3.5%Al-1%Zn-1%Sn-1%Ce-0.1%Mn alloy anode. In this work, NaF with different concentrations as the electrolyte additives were added into 0.7 mol L^{-1} NaCl. The investigated concentrations were 0, 0.1, 0.5, 0.8, 1.0 and 2.0 mmol L^{-1}, respectively. The results of a series of electrochemical tests demonstrated that the current density of the anode was much higher in

the electrolyte with 0.8 mmol L^{-1} NaF addition. And the optimum concentration of the NaF addition was 0.8 mmol L^{-1}, which greatly improved the discharge activity of the anode. Subsequently, a Mg/H_2O_2 fuel cell was assembled with nickel foam-supported Pd as the cathode while the prepared magnesium alloy as the anode. The peak power density of the assembled Mg/H_2O_2 fuel cell with NaF addition reached 77 mW cm^{-2}, while the value was only 62 mW cm^{-2} without NaF addition. The increase was even as high as 24%.

4.5 First-principles calculations

There have been extensive experimental researches of the corrosion behavior of metals and alloys. First-principles calculations have attracted an increasing attention in predicting the properties of varieties of materials since its first appearance [103-105]. In terms of metals and alloys, first-principles calculations have been applied to aluminum alloys to present a theoretical assessment of galvanic corrosion by calculating the work function (φ) based on density functional theory (DFT) [106, 107]. It is known to all that the second phases played a vital role in the electrochemical and corrosion properties of alloy. For example, common β-$Mg_{17}Al_{12}$ second phases in magnesium alloys have two effects on their corrosion resistance, one is a cathode phase to promote the galvanic corrosion while the other as a barrier for restricting the corrosion, which largely relies on its volume fraction and distribution in the magnesium matrix [90, 91, 108]. Jin et al. [106] used the first-principles calculations to predict the volta potential difference between the second phases and the matrix, whose results were well associated with the experimental results. Obviously, the smaller the volta potential difference is, the weaker the galvanic corrosion will be. Qin et al. [107] carried out the similar theoretical calculations. An ab-initio study was implemented to reveal the role of Mg_2Si and Al_2CuMg phases in corrosion behavior of Al alloys. As the results showed, the two phases could serve as cathode or anode, strengthening or weakening the local galvanic corrosion of the metal matrix, respectively.

Obviously, first-principle calculations can provide theoretical basis for experiments, and even provide guidance for the research of high-performance magnesium alloys anodes, shortening the development cycle and saving the experimental costs. It is of great significance to combine this theory with practice and has developed into a trend.

Chen et al. [109] innovatively reported the theoretical limits to the anode potential of Mg-air batteries. A DFT method was used in this work to calculate the free energies of intermediate reactions and the overall free energy change was obtained to investigate the dissolution process of magnesium, and a hydroxide-assisted anodic dissolution mechanism was then put forward. The results showed that only the electrochemical reactions that occurred on the surface in the dissolution process could decide the theoretical limiting potential of magnesium. It was also concluded that the battery cannot obtain a higher potential even if corrosion was completely suppressed due to the appearance of $Mg(OH)_2$ passivation film, which enhanced the net corrosion potential.

Zhang et al. [110] implemented the first-principles research for seeking alloying elements that could increase the corrosion resistance of magnesium. It is widely accepted that the coupling of anodic magnesium dissolution and cathodic hydrogen evolution on the impurity like nickel (Ni) and copper

(Cu) particles triggered the galvanic corrosion. In this work, a method of high-throughput DFT computations was implemented to screen out a group of elements that could segregate from the bulk magnesium to the surfaces of nickel or copper impurities and hinder the HER. They concluded that the six p-block elements could meet the needs. The ability to restrict the HER ranked as follows: Al≈ P< Ga< Si< Ge< As. As and Ge were the best of all 68 calculated elements to restrict the HER on the surface of Ni particles. Similar calculations were also performed on the surface of Cu. However, the effect of the six elements to reduce the HER on Cu surface was constricted due to their poor stability on Cu surface. Relying on the surface concentration of As, the energies of hydrogen adsorption could be greatly reduced, which could reduce the generation of the adsorbed hydrogen atoms through the dissociation of water.

5. CONCLUSIONS AND PROSPECTS

With the growing demand for chemical power supplies with excellent electrochemical properties and stability used in both long-duration low-power and short-term high-power applications, magnesium metal has attracted enough attention due to its numerous inherent advantages used as the anodes for varieties of batteries. Magnesium as the anodes has been successfully applied in air batteries, seawater batteries, fuel cells, primary batteries and second batteries. However, some problems of the magnesium material restrict its further application as the anodes. The formation of $Mg(OH)_2$ passivation film detrimentally reduces the discharge activity of magnesium, besides, it undergoes severe self-corrosion in the process of discharge, which results in a low anodic efficiency. Considering these shortcomings, it has become an urgent topic to develop such a magnesium anode with both high discharge activity and good corrosion resistance simultaneously.

The methods to improve the performance of magnesium as anodes in recent years have been reviewed. Usually, the methods include alloying, heat treatment, plastic deformation and electrolyte optimization. These methods either accelerate the self-exfoliation of the discharge products, or impair the HER process in the course of discharge, or refine the microstructure or reduce the galvanic corrosion by the effect of new second phases, all of which lead to an improvement of the anode performance. In recent years, a new approach of first-principles calculations has become more and more seductive and been used to theoretically explain the changes in discharge activity and corrosion behavior.

Various methods have been applied to improve the performance of magnesium anodes, with alloying, heat treatment and subsequent plastic deformation treatment widely used up to now. Obviously, it is of great significance to develop such a kind of magnesium alloy anode with both high discharge activity and simultaneous low self-corrosion rate by combining these methods. It is also an interesting subject to use the first- principles calculations for the theoretical explanation and the prediction of research direction in the further.

ACKNOWLEDGEMENTS
The authors acknowledge the financial support of Key Laboratory of Metal Fuel Cell of Sichuan Province.

References

1. H. Zhao, P. Bian and D. Ju, *J. Environ. Sci.*, 21 (2009) S88.
2. S. M. He, X. Q. Zeng, L. M. Peng, X. Gao, J. F. Nie and W. J. Ding, *J. Alloy. Compd.*, 427 (2007) 316.
3. Y. Hu, J. Deng, C. Zhao, J. Wang and F. Pan, *Trans. Nonferrous Met. Soc. China*, 21 (2011) 732.
4. Y. a. Chen, J. Gao, Y. Song and Y. Wang, *Mater. Sci. Eng.*, A, 671 (2016) 127.
5. Y. Hu, C. Zhang, W. Meng, F. Pan and J. Zhou, *J. Alloy. Compd.*, 727 (2017) 491.
6. T. Zhang, Z. Tao and J. Chen, *Mater. Horiz.*, 1 (2014) 196.
7. Y. Ma, N. Li, D. Li, M. Zhang and X. Huang, *J. Power Sources*, 196 (2011) 2346.
8. T. Zheng, Y. Hu, Y. Zhang, S. Yang and F. Pan, *Mater. Des.*, 137 (2018) 245.
9. N. Wang, R. Wang, C. Peng, B. Peng, Y. Feng and C. Hu, *Electrochim. Acta*, 149 (2014) 193.
10. Y. Koo, J. Sankar and Y. Yun, *Biomicrofluidics*, 8 (2014) 054104.
11. S. Deng, D. Yi, L. Zhao, L. Zhou, B. Wang, C. Ji and B. Lan, *Chin. J. Power Sources*, 31 (2007) 402.
12. T. Khoo, A. Somers, A. A. J. Torriero, D. R. MacFarlane, P. C. Howlett and M. Forsyth, *Electrochim. Acta*, 87 (2013) 701.
13. J. Zhao, K. Yu, Y. Hu, S. Li, X. Tan, F. Chen and Z. Yu, *Electrochim. Acta*, 56 (2011) 8224.
14. R. Udhayan, N. Muniyandi and P. B. Mathur, *Br. Corros. J.*, 27 (1992) 68.
15. N. Wang, R. Wang, C. Peng, C. Hu, Y. Feng and B. Peng, *Trans. Nonferrous Met. Soc. China*, 24 (2014) 2427.
16. D. Cao, L. Wu, G. Wang and Y. Lv, *J. Power Sources*, 183 (2008) 799.
17. D. Cao, L. Wu, Y. Sun, G. Wang and Y. Lv, *J. Power Sources*, 177 (2008) 624.
18. M. Deng, D. Höche, S. V. Lamaka, D. Snihirova and M. L. Zheludkevich, *J. Power Sources*, 396 (2018) 109.
19. Y. Li and J. Lu, *ACS Energy Lett.*, 2 (2017) 1370.
20. M. Armand and J. M. Tarascon, *Nature*, 451 (2008) 652.
21. F. Cheng and J. Chen, *Chem. Soc. Rev.*, 41 (2012) 2172.
22. Ø. Hasvold, T. Lian, E. Haakaas, N. Størkersen, O. Perelman and S. Cordier, *J. Power Sources*, 136 (2004) 232.
23. M. A. Rahman, X. Wang and C. Wen, *J. Electrochem. Soc.*, 160 (2013) A1759.
24. M. Nestoridi, D. Pletcher, R. J. K. Wood, S. Wang, R. L. Jones, K. R. Stokes and I. Wilcock, *J. Power Sources*, 178 (2008) 445.
25. J.-S. Lee, S. Tai Kim, R. Cao, N.-S. Choi, M. Liu, K. T. Lee and J. Cho, *Adv. Energy Mater.*, 1 (2011) 34.
26. C. W. Lee, K. Sathiyanarayanan, S. W. Eom and M. S. Yun, *J. Power Sources*, 160 (2006) 1436.
27. J. Ma, G. Wang, Y. Li, W. Li and F. Ren, *J. Mater. Eng. Perform.*, 27 (2018) 2247.
28. X. Li, H. Lu, S. Yuan, J. Bai, J. Wang, Y. Cao and Q. Hong, *J. Electrochem. Soc.*, 164 (2017) A3131.
29. S. Yuan, H. Lu, Z. Sun, L. Fan, X. Zhu and W. Zhang, *J. Electrochem. Soc.*, 163 (2016) A1181.

30. J. Kubasek, D. Vojtech, J. Lipov and T. Ruml, *Mater. Sci. Eng.*, C, 33 (2013) 2421.
31. S. M. Hwang, J. S. Park, Y. Kim, W. Go, J. Han, Y. Kim and Y. Kim, *Adv Mater*, 31 (2019) e1804936.
32. N. Wang, R. Wang, C. Peng, Y. Feng and X. Zhang, *Trans. Nonferrous Met. Soc. China*, 20 (2010) 1403.
33. M. Shinohara, E. Araki, M. Mochizuki, T. Kanazawa and K. Suyehiro, *J. Power Sources*, 187 (2009) 253.
34. K. V. Rao, *Defen. Sci. J.*, 51 (2001) 161.
35. R. Renuka, *J. Appl. Electrochem*., 29 (1999) 271.
36. K. Yu, X. Tan, Y. Hu, F. Chen and S. Li, *Corros. Sci*., 53 (2011) 2035.
37. R. Wang, Q. Li, N. Wang, C. Peng and Y. Feng, *J. Mater. Eng. Perform.*, 27 (2018) 6552.
38. F. Sammoura, K. B. Lee and L. Lin, *Sens. Actuators*, A, 111 (2004) 79.
39. W. S. D. Wilcock and P. C. Kauffman, *J. Power Sources*, 66 (1997) 71.
40. R. Balasubramanian, A. Veluchamy, N. Venkatakrishnan and R. Gangadharan, *J. Power Sources*, 56 (1995) 197.
41. Y. Jiang, *Marine Electric & Electric Technology*, 5 (2005) 46.
42. W. Jiao, Y. Fan, C. Huang and Sanglin, *Ionics*, 24 (2017) 285.
43. J. Park, J. Park, S. T. Senthilkumar and Y. Kim, *J. Power Sources*, 450 (2020).
44. X. Liu, J. Xue and S. Liu, *Mater. Des.*, 160 (2018) 138.
45. Ø. Hasvold and N. Størkersen, *J. Power Sources*, 96 (2001) 252.
46. Ø. Hasvold, H. Henriksen, E. Melvær, G. Citi, B. Ø. Johansen, T. Kjønigsen and R. Galetti, *J. Power Sources*, 65 (1997) 253.
47. J. S. Lauer, J. F. Jackovitz and E. S. Buzzelli, *J. Electrochem. Soc*., 34 (1990) 115.
48. C. Shu, E. Wang, L. Jiang, Q. Tang and G. Sun, *J. Power Sources*, 208 (2012) 159.
49. Y. Lv, Y. Xu and D. Cao, *J. Power Sources*, 196 (2011) 8809.
50. Ø. Hasvold, N. J. Størkersen, S. Forseth and T. Lian, *J. Power Sources*, 162 (2006) 935.
51. N. Størkersen and Ø. Hasvold, *Science and Defence Conf*, (2004) 1.
52. M. G. Medeiros and E. G. Dow, *J. Power Sources*, 80 (1999) 78.
53. M. G. Medeiros, R. R. Bessette, C. M. Deschenes and D. W. Atwater, *J. Power Sources*, 96 (2001) 236.
54. N. Munichandraiah, *J. Appl. Electrochem*., 29 (1999) 463.
55. S. U. Kim and C. W. Monroe, *Appl. Energy*, 103 (2013) 207.
56. J. Xu, Q. Yang, C. Huang, M. S. Javed, M. K. Aslam and C. Chen, *J. Appl. Electrochem.*, 47 (2017) 767.
57. J. Xu, Q. Yang, M. S. Javed, Y. Gong, M. K. Aslam and C. Chen, *RSC Advances*, 7 (2017) 5880.
58. S. Mohanraj, (2016).
59. Z. Ma, M. Forsyth, D. R. MacFarlane and M. Kar, *Green Energy Environ*., 4 (2019) 146.
60. Z. Zhang, S. Dong, Z. Cui, A. Du, G. Li and G. Cui, *Small Methods*, 2 (2018).
61. J. F. Wishart, *Energy Environ. Sci.*, 2 (2009) 956.
62. T. D. Gregory, R. J. Hoffman and R. C. Winterton, *J. Electrochem. Soc.*, 137 (1990) 775.
63. T. Kakibe, J. Hishii, N. Yoshimoto, M. Egashira and M. Morita, *J. Power Sources*, 203 (2012) 195.
64. Y. Xiao, M. Pan, J. Zou, R. Guo, X. Zeng and W. Ding, *Ionics*, 25 (2019) 5889.
65. A. K. Padhi, *J. Electrochem. Soc.*, 144 (1997) 1188.
66. G. Gershinsky, H. D. Yoo, Y. Gofer and D. Aurbach, *Langmuir*, 29 (2013) 10964.
67. Y. Liang, R. Feng, S. Yang, H. Ma, J. Liang and J. Chen, *Adv Mater*, 23 (2011) 640.
68. I. Shterenberg, M. Salama, Y. Gofer, E. Levi and D. Aurbach, *MRS Bull.*, 39 (2014) 453.

69. M. Liu, P. Schmutz, S. Zanna, A. Seyeux, H. Ardelean, G. Song, A. Atrens and P. Marcus, *Corros. Sci.,* 52 (2010) 562.
70. J. Liao and M. Hotta, *Corros. Sci.,* 112 (2016) 276.
71. N. Wang, R. Wang, C. Peng, Y. Feng and B. Chen, *Corros. Sci.,* 64 (2012) 17.
72. N. Wang, R. Wang, C. Peng and Y. Feng, *Corros. Sci.,* 81 (2014) 85.
73. M. C. Lin, C. Y. Tsai and J. Y. Uan, *Corros. Sci.,* 51 (2009) 2463.
74. L. Wen, K. Yu, H. Xiong, Y. Dai, S. Yang, X. Qiao, F. Teng and S. Fan, *Electrochim. Acta,* 194 (2016) 40.
75. Y. Feng, L. Liu, R. Wang, C. Peng and N. Wang, *Trans. Nonferrous Met. Soc. China,* 26 (2016) 1379.
76. L. Wang, R. Wang, Y. Feng, M. Deng and N. Wang, *J. Electrochem. Soc.,* 164 (2017) A438.
77. R. Zeng, J. Zhang, W. Huang, W. Dietzel, K. U. Kainer, C. Blawert and W. Ke, *Trans. Nonferrous Met. Soc. China,* 16 (2006) s763.
78. A. Pardo, M. C. Merino, A. E. Coy, R. Arrabal, F. Viejo and E. Matykina, *Corros. Sci.,* 50 (2008) 823.
79. K. Yu, H. Xiong, L. Wen, Y. Dai, S. Yang, S. Fan, F. Teng and X. Qiao, *Trans. Nonferrous Met. Soc. China,* 25 (2015) 1234.
80. J. Li, K. Wan, Q. Jiang, H. Sun, Y. Li, B. Hou, L. Zhu and M. Liu, *Metals*, 6 (2016) 65.
81. X. Zhao, J. Su, G. Li, J. He, S. Chen, G. Wang and A. Liu, *Mater. Corros.,* 70 (2019) 2082.
82. N. Birbilis, M. K. Cavanaugh, A. D. Sudholz, S. M. Zhu, M. A. Easton and M. A. Gibson, *Corros. Sci.,* 53 (2011) 168.
83. T. Zhang, G. Meng, Y. Shao, Z. Cui and F. Wang, *Corros. Sci.,* 53 (2011) 2934.
84. Y. Feng, W. Xiong, J. Zhang, R. Wang and N. Wang, *J. Mater. Chem.* A, 4 (2016) 8658.
85. N. Wang, R. Wang, Y. Feng, W. Xiong, J. Zhang and M. Deng, *Corros. Sci.,* 112 (2016) 13.
86. H. Xiong, H. Zhu, J. Luo, K. Yu, C. Shi, H. Fang and Y. Zhang, *J. Mater. Eng. Perform.,* 26 (2017) 2901.
87. L. Wang, R. Wang, Y. Feng, M. Deng and N. Wang, *JOM*, 69 (2017) 2467.
88. H. Xiong, K. Yu, X. Yin, Y. Dai, Y. Yan and H. Zhu, *J. Alloy. Compd.,* 708 (2017) 652.
89. Y. Lv, M. Liu, Y. Xu, D. Cao and J. Feng, *J. Power Sources*, 225 (2013) 124.
90. N. Wang, R. Wang, C. Peng and Y. Feng, *J. Mater. Eng. Perform.,* 21 (2011) 1300.
91. G. Song, A. Atrens and M. Dargusch, *Corros. Sci.,* 41 (1998) 249.
92. M. Ben Haroush, G. Ben Hamu, D. Eliezer and L. Wagner, *Corros. Sci.,* 50 (2008) 1766.
93. G. B. Hamu, D. Eliezer and L. Wagner, *J. Alloy. Compd.,* 468 (2009) 222.
94. G. Song, R. Mishra and Z. Xu, *Electrochem. Commun.,* 12 (2010) 1009.
95. Y. Shi, C. Peng, Y. Feng, R. Wang and N. Wang, *J. Alloy. Compd.,* 721 (2017) 392.
96. D. Song, A. B. Ma, J. H. Jiang, P. H. Lin, D. H. Yang and J. F. Fan, *Corros. Sci.,* 53 (2011) 362.
97. Z. Shi, M. Liu and A. Atrens, *Corros. Sci.,* 52 (2010) 579.
98. N. Wang, R. Wang, C. Peng, B. Peng, Y. Feng and C. Hu, *J. Mater. Eng. Perform.,* 23 (2014) 4374.
99. N. Wang, Y. Mu, Q. Li and Z. Shi, *RSC Advances*, 7 (2017) 53226.
100. J. Wu, R. Wang, Y. Feng and C. Peng, *J. Alloy. Compd.,* 765 (2018) 736.
101. Y. Li, J. Ma, G. Wang, F. Ren, Y. Zhu and Y. Song, *J. Electrochem. Soc.,* 165 (2018) A1713.
102. Y. Lv, D. Tang, D. Cao, G. Wang, M. Zhang and J. Feng, *RSC Advances*, 5 (2015) 46423.
103. Y. Z. Ji, A. Issa, T. W. Heo, J. E. Saal, C. Wolverton and L. Q. Chen, *Acta Mater.*, 76 (2014) 259.
104. Q. Chen, Z. Huang, Z. Zhao and C. Hu, *Comput. Mater. Sci.,* 67 (2013) 196.
105. X. Tao, Y. Ouyang, H. Liu, Y. Feng, Y. Du, Y. He and Z. Jin, *J. Alloy. Compd.,* 509 (2011) 6899.
106. Y. Jin, M. Liu, C. Zhang, C. Leygraf, L. Wen and J. Pan, *J. Electrochem. Soc.,* 164 (2017) C465.

107. Y.-F. Qin and S.-Q. Wang, *J. Electrochem. Soc*., 162 (2015) C503.
108. G. Song, A. L. Bowles and D. H. StJohn, *Mater. Sci. Eng*., A, 366 (2004) 74.
109. L. D. Chen, J. K. Nørskov and A. C. Luntz, *J. Phys. Chem*. C, 119 (2015) 19660.
110. M. Zhang, L. G. Hector, Y. Guo, M. Liu and L. Qi, *Comput. Mater. Sci*., 165 (2019) 154